Xu *et al. Energy Mater* 2024;4:400034
DOI: 10.20517/energymater.2023.86

Energy Materials

Article

Open Access

Check for updates

Evolved photovoltaic performance of $MAPbI_3$ and $FAPbI_3$-based perovskite solar cells in low-temperatures

Youcheng Xu[1,#], Ziyi Wu[1,#], Ziling Zhang[1], Xin Li[2,*], Hong Lin[1,*]

[1]State Key Laboratory of New Ceramics and Fine Processing, School of Materials Science and Engineering, Tsinghua University, Beijing 100084, China.
[2]School of Electronic Science and Engineering, Xiamen University, Xiamen 361005, China.
[#]Authors contributed equally.

[*]**Correspondence to:** Prof. Xin Li, School of Electronic Science and Engineering, Xiamen University, Xiamen 361005, China. E-mail: lixin01@xmu.edu.cn; Prof. Hong Lin, School of Materials Science and Engineering, Tsinghua University, Beijing, 100084, China. E-mail: hong-lin@tsinghua.edu.cn

How to cite this article: Xu Y, Wu Z, Zhang Z, Li X, Lin H. Evolved photovoltaic performance of $MAPbI_3$ and $FAPbI_3$-based perovskite solar cells in low-temperatures. *Energy Mater* 2024;4:400034. https://dx.doi.org/10.20517/energymater.2023.86

Received: 31 Oct 2023 **First Decision:** 28 Dec 2023 **Revised:** 8 Mar 2024 **Accepted:** 21 Mar 2024 **Published:** 15 Apr 2024

Academic Editor: Meicheng Li **Copy Editor:** Dong-Li Li P**roduction Editor:** Dong-Li Li

Abstract

Organic-inorganic hybrid perovskites have emerged as an up-and-coming contender for photovoltaic devices owing to their exceptional photovoltaic properties. However, current research predominantly concentrates on their performance under ambient conditions at room temperature. In this work, we delve into the novel territory by investigating $MAPbI_3$-based and $FAPbI_3$-based perovskite solar cells (PSCs) in the temperature range of 300 to 150 K. Remarkable efficiency enhancements of nearly 5% and 20% were obtained at 250 and 210 K, respectively. However, further decreasing the temperature impairs the photovoltaic performance. We propose an underlying mechanism influencing the performance change in perovskite devices at low temperatures by examining the temperature-dependent ultraviolet-visible and photoluminescence spectra results. At the beginning of the cooling process, from 300 to 250 K for $MAPbI_3$ and from 300 to 210 K for $FAPbI_3$, the performance enhancement stems primarily from the enhanced open-circuit voltage by the tuned band gap of the perovskite films. Further lowering the temperature would change the perovskite structure, impairing the performance of PSCs. $FAPbI_3$-based PSCs show a better tolerance in low temperatures owing to the more stable perovskite crystal structure. The present findings offer valuable theoretical guidance for preparing outstanding PSCs for low-temperature applications.

Keywords: Perovskite solar cells, low temperature, phase transition, defective state, carrier trapping

© The Author(s) 2024. **Open Access** This article is licensed under a Creative Commons Attribution 4.0 International License (https://creativecommons.org/licenses/by/4.0/), which permits unrestricted use, sharing, adaptation, distribution and reproduction in any medium or format, for any purpose, even commercially, as long as you give appropriate credit to the original author(s) and the source, provide a link to the Creative Commons license, and indicate if changes were made.

INTRODUCTION

The organic-inorganic perovskite solar cell (PSC), described as ABX_3, holds significant promise due to its tunable photoelectric properties and extended carrier lifetime[1], in which A represents monovalent cations such as formamidine cation (FA^+) and methylamine cation (MA^+), B typically denotes Pb^{2+} or Sn^{2+}, and X signifies halide anion Cl^-, Br^- and I^-. Since the pioneer work of Dieter Weber on the three-dimensional MAPbX3 PSC in 1978[2], persistent endeavors have been dedicated to refining the formula and enhancing the process, resulting in notable advancements such as achieving a remarkable 26.1% power conversion efficiency (PCE)[3]. At the same time, researchers are continually proposing methods that can further improve the performance of perovskite cells, such as employing small fluorinated organic ammonium molecules to compensate for the pinholes and cracks in perovskites to achieve high-quality perovskite films with larger grain sizes and lower crystal defect densities[4] or using $InBr_3$ modifications to construct homojunctions to expand the electric field and enhance device performance[5].

Perovskites are renowned for their remarkable photoelectric properties at room temperature, prompting interest in their applicability in low-temperature environments such as polar regions and terrestrial space. However, such extreme conditions can lead to decreased efficiency and irreversible damage to photovoltaic cells. For instance, current spacecraft solar cells predominantly employ silicon and GaAs. Measured parameters under the air mass 1.5 global (AM 1.5G) spectrum (1,000 W/m^2) at 25 °C reveal the highest PCE of 37.9% and open-circuit voltage (V_{OC}) of 3.06V[6] of GaAs, alongside peak short-circuit current (J_{SC}) for 42.62 mA/cm^2 of single crystal Si[7]. In comparison, organic-inorganic perovskites show average parameters in PCE, V_{OC} and J_{SC}. However, they exhibit a high absorption coefficient, impressive mechanical flexibility and radiation tolerance, positioning them as excellent candidates for spacecraft solar systems.

Recently, there has been a growing exploration of perovskite performance in low-temperature conditions, unveiling its potential for development. In a study by Chen *et al.*, conventional n-i-p planar solar cell employing $(FA,MA,Cs)Pb(I,Br)_3$ (FAMACs)-based perovskite materials achieved a remarkable 25.2% efficiency at 220 K, showing an increasing PCE trend from 300 to 220 K, followed by a decline as temperature further decreased to 130 K[8]. Similar trends were observed in the V_{OC} and hysteresis index, but no change was noted in Jsc density across the temperature range. A theory proposing a transition activating the self-elimination of the intrinsic defect was introduced to explain these results, later validated through density functional theory (DFT) calculations.

Herein, we delve into FA-based and MA-based PSCs across varying operational temperatures (300 to 150 K) and explore $FAPbI_3$ and $MAPbI_3$ perovskite films from 300 to 100 K. Notably, we observed an enhancement in PCE and V_{OC} for both FA and MA solar cells, albeit occurring at different temperature points. To comprehensively understand these variations, temperature-dependent steady-state photoluminescence (PL) measurements and temperature-dependent ultraviolet-visible (UV-vis) transmittance spectra measurements were also conducted to explore the change in bandgap and photovoltaic behavior. Notably, distinct discrepancies emerged between FA- and MA-based perovskites. This investigation uncovers a correlation between perovskite bandgap behavior and device performance.

EXPERIMENTAL

Materials

Herein, all the materials were purchased from Sigma-Aldrich or Alfa-Aesar and used without further purification. Ethanol (anhydrous) and isopropyl alcohol (> 99.7%) were purchased from Greagent. PbI2 (99.99%) was bought from Tokyo Chemical Industry (TCI). Formamidinium iodide (FAI) (> 99.99%), methylammonium iodide (MAI) (> 99.99%), and methylammonium bromide (MABr) (> 99.99%) were

purchased from Greatcell Solar. Spiro-OMeTAD (99.7%) was bought from Borun Chemical Co., Ltd. All the materials were used as received without purification.

Materials synthesis

Fabrication of solar cells. Substrates were cleaned in deionized water, ethanol, acetone, and isopropyl alcohol in sequence and treated with O_2-plasma for 15 min to remove organic contamination and construct a hydrophilic interface. The SnO_2 nanoparticle dispersion obtained was spun on the cleaned indium tin oxide-coated glass substrate at 4,000 rpm for 30 s, followed by annealing at 150 °C for 40 min. The $FAPbI_3$ perovskite was deposited using a two steps program at 1,000 rpm for 10 s in the first step and 5,000 rpm for 30 s in the second, during which diethyl ether was dropped onto the center of the substrate at 22 s after the start of the procedure. The $MAPbI_3$ perovskite was deposited employing a two-step program at 1,000 rpm for 10 s in the first step and 4,000 rpm for 40 s in the second, during which diethyl ether was dropped onto the center of the substrate at 10 s before the end of the procedure. Subsequently, the hole transporting material Spiro-OMeTAD was spun on the perovskite film at 3,000 rpm for 30 s. Finally, 100 nm gold electrodes were deposited on substrates through thermal evaporation.

Fabrication of perovskite films. The $FAPbI_3$ and $MAPbI_3$ perovskite film for characterization was deposited on SnO_2 spun indium tin oxide-coated glass substrate with the same procedure above.

Characterization

The current density-voltage (J-V) curves for all devices at room temperature were carried out with a digital source meter (2400, Keithley Instruments, USA) scanning from -0.1 to 1.3 V at a scan rate of 0.05 $V \cdot s^{-1}$ under AM 1.5G illumination (100 $mW \cdot cm^{-2}$) with a 0.06 cm^2 metal mask over, which was realized using a solar simulator (Oriel, USA, calibrated with a standard crystalline silicon solar cell). The temperature-dependent J-V curves were measured by a solar simulator (Newport, USA) while samples were put in a hermetic probe station connected to a digital source meter (2400, Keithley Instruments, USA).

The morphology of perovskite samples was characterized by a scanning electron microscope (SEM) (Zeiss, LEO1530, Germany). Temperature-dependent steady-state PL measurements were conducted in a step of 2 nm by exciting the sample with a monochromatic xenon lamp (central wavelength λ = 460 nm) under a position of a 45° angle towards the excitation beam. The sample stage was kept in a hermetic and vacuum environment with a temperature control system. Temperature-dependent UV-vis transmittance spectra were performed using a Lambda 950 spectrophotometer (PerkinElmer, USA), sharing the same temperature control system with the PL test. Temperature-dependent Raman spectra measurements were recorded on a laser micro-Raman spectroscope (Horiba Jobin Yvon, Hr800, France) with a laser beam wavelength of 532 nm for the $MAPbI_3$ perovskite film and a 633 nm laser beam for the $FAPbI_3$ film.

RESULTS AND DISCUSSION

We first observed the surface morphology of $MAPbI_3$ and $FAPbI_3$ perovskite thin films prepared on SnO_2 substrates using SEM, as shown in Figure 1, where a represents the $MAPbI_3$ sample, and b indicates the $FAPbI_3$ sample. It can be observed that, at room temperature, both types of perovskite thin films exhibit good uniformity, and no pores are present on the surface of the films. The grain size distribution of the $FAPbI_3$ film is broader, with the largest size approaching 1.9 μm; the grain sizes in the $MAPbI_3$ film are more similar, not exceeding 500 nm.

We then studied the change of the UV-vis spectra of the polycrystalline perovskite films employing a cooling process from 300 to 110 K [Figure 2]. $CH_3NH_3PbI_3$ (MAPI) and $CH(NH_2)_2PbI_3$ (FAPI) were

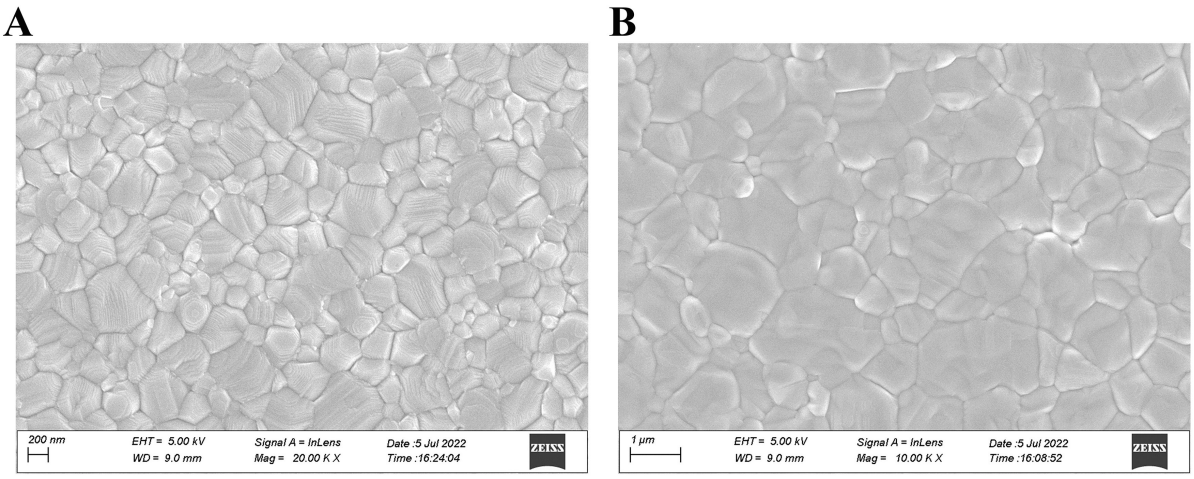

Figure 1. The morphology of perovskite films at room temperature: (A) $MAPbI_3$ film; (B) $FAPbI_3$ film.

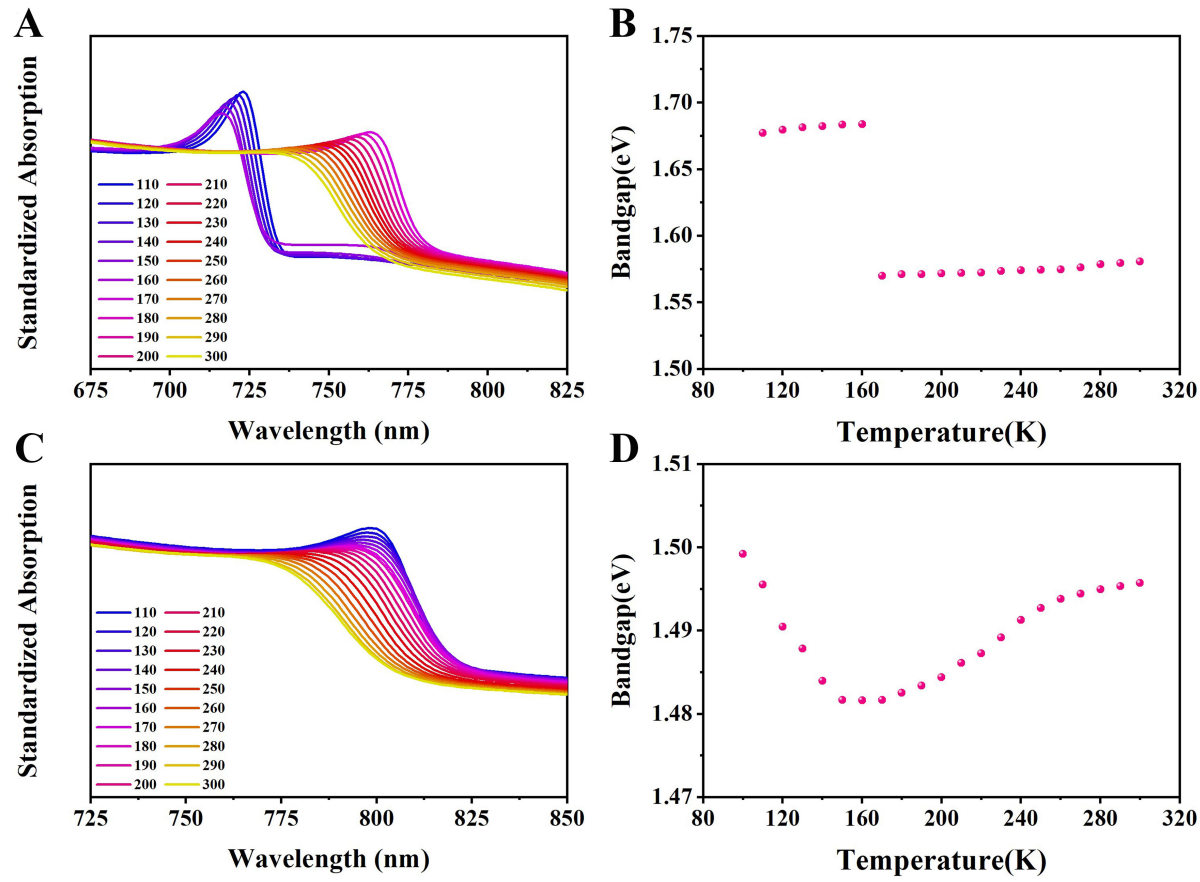

Figure 2. Temperature-dependent UV-vis spectra for (A and B) $MAPbI_3$ and (C and D) $FAPbI_3$ with their calculated bandgaps in different temperatures. UV-vis: Ultraviolet-visible.

deposited onto SnO_2-obtained indium tin oxide (ITO) glass. As the high transparency of the SnO_2 film is above the 400 nm range[9], it has negligible impact on spectral pattern. Therefore, any disparities observed in the spectra can be attributed to perovskite behavior. Figure 2A presents the $MAPbI_3$ spectra spanning from

675 to 825 nm. Notably, a distinct peak emerges at approximately 770 nm when measured at 170 K, which is a manifestation of excitonic transition. The peak position also shifts towards shorter wavelengths as the temperature increases, frequently observed in lead composite semiconductors[10]. However, at 300 K, discerning this peak from the conduction band continuum becomes challenging. Another interesting thing is that an excitonic peak at around 715 nm occurs when measured at 160 K. As the temperature further decreased, there was a sudden jump of the peak towards longer wavelengths. This behavior can be attributed to a tetragonal-to-orthorhombic phase transition occurring near 160 K[11].

With detailed calculation shown in Supplementary Figure 1, Figure 2B shows the calculated band gap of $MAPbI_3$, where we can observe a positive thermal expansion coefficient of its band gap in both tetragonal and orthorhombic structures besides a sudden jump at the phase-transition point of 170 K. However, it is raised that inorganic semiconductors, such as silicon and germanium, have an increase in their band gap as temperature goes down due to the change of electron-phonon interaction[12]. One theory to explain such abnormal positive thermal expansion coefficient in tetragonal and orthorhombic structure phases is that a photon mode, Pb-I-Pb angular bending vibration, may contribute to the position of the band gap by thermal population as the position of the conduction and valence bands in a semiconductor is decided by phonon populations at specific temperature[11]. First-principles calculation of band gap in other research shows that tetragonal and orthorhombic $MAPbI_3$ perovskite has 1.60 and 1.82 eV bandgaps, respectively, which is reflected well by the calculated bandgaps in Figure 2B[13]. The energy rise in σ-antibonding orbitals of Pb and I may lead to a narrow bandwidth[14].

Figure 2C illustrates the spectra of the $FAPbI_3$ perovskite film at different temperatures. Compared to those of $MAPbI_3$, it exhibits a similar pattern at 300 K. The featuring peak demonstrates a similar shift towards longer wavelengths when the temperature falls. When the temperature reaches and goes below 160 K, $FAPbI_3$ displays a slight bump, possibly due to a small crystal-structure transient. A previous study indicated that there might be a transition from the tetragonal (I) phase to the tetragonal (II) phase when a more subtle alteration in the chemical and structural environment happens[15]. In this case, $FAPbI_3$ perovskite shows similarity in its tetragonal (I) phase. Still, it undergoes a continuous change and an inverse negative thermal expansion coefficient in the tetragonal (II) phase [Figure 2D]. Such a phenomenon requires further research.

Additionally, we used SEM to observe the microstructure of $MAPbI_3$ thin film samples just after completing the cooling process [Supplementary Figure 2]. Compared to the SEM photos taken before cooling, the previously uniform sample films showed a greater number of pores after the cooling process. We speculate that the phase transition-induced change in lattice size during cooling reduces grain size. Although the temperature is restored during observation under room temperature SEM, the size changes caused by the phase transition, influenced by spatial orientation, cannot fully revert. This results in the observation of numerous pores on the sample films.

The changed energetic structure of $MAPbI_3$ and $FAPbI_3$ films would directly affect the photon-generating carrier dynamics, such as the exciton physics. Herein, we performed temperature-dependent steady-state PL measurements to explore the evolving optoelectronic properties of $MAPbI_3$ and $FAPbI_3$ films. Figure 3A and B summarizes the temperature-dependent PL spectra for $MAPbI_3$ film. Colorful mapping of normalized PL spectra in different temperatures is depicted in Figure 3A to reveal the change of emission peak, with the central positions in Figure 3B. At 300 K, only one peak appears at the wavelength of nearly 780 nm. When the temperature declines, the high-temperature peak (line Peak 2) exhibits a continuous shift towards longer wavelengths in its position before 160 K and shrinks in width. This shifting tendency in position from 290 to 160 K is consistent with the decreasing band gap calculated in Figure 2B.

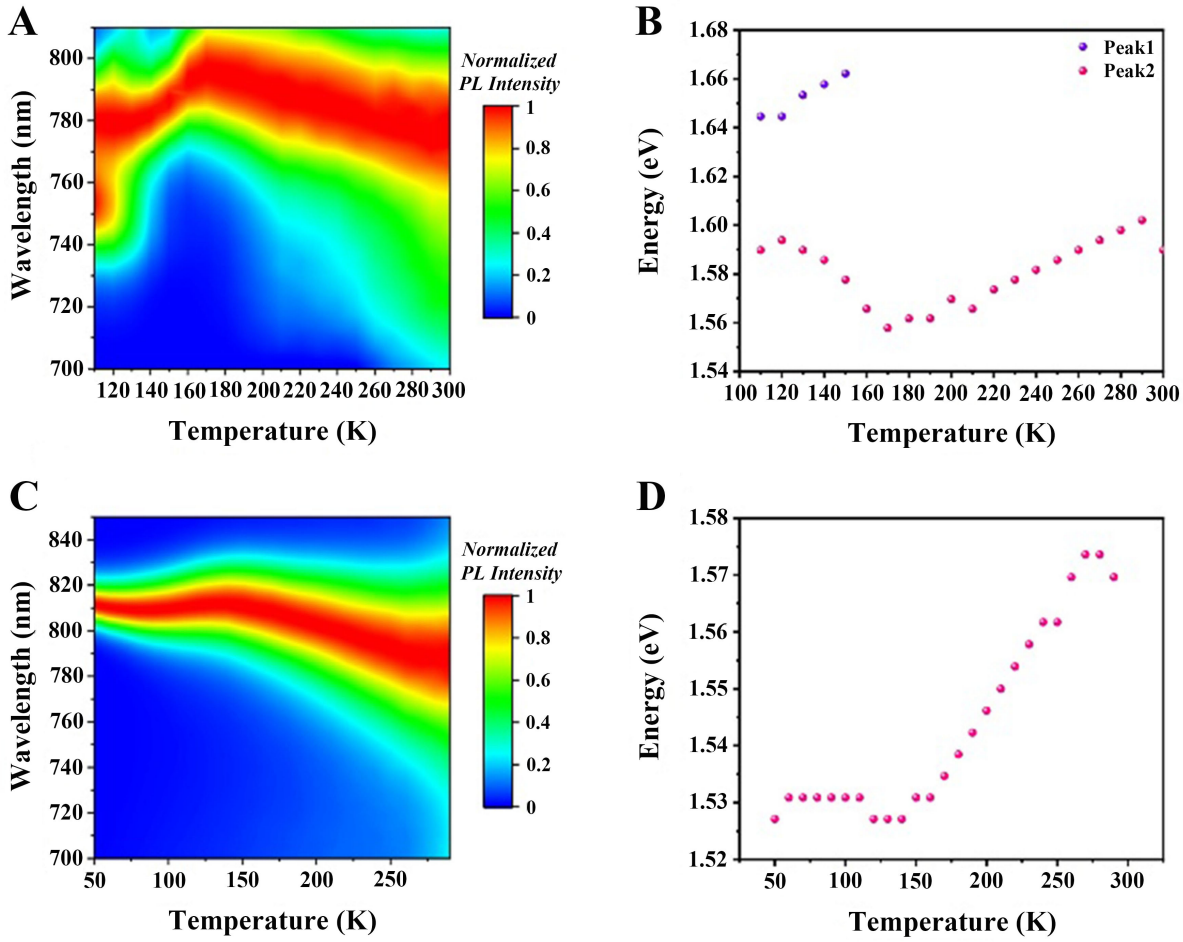

Figure 3. Temperature-dependent photoluminescence spectra for $MAPbI_3$ and $FAPbI_3$. (A) Color plots of normalized PL spectra for $MAPbI_3$-based perovskites at different temperatures from 110 to 300 K; (B) The corresponding excitonic peak positions of $MAPbI_3$-based perovskites; (C) Color plots of normalized PL spectra for $FAPbI_3$-based perovskites at varying temperatures from 50 to 290 K (D) The corresponding excitonic peak position of the $FAPbI_3$-based perovskites. PL: Photoluminescence.

However, two PL peaks are observed when the temperature goes down below 150 K [Figure 3B]. Then, the long-wavelength peak showcases a shift tendency towards shorter wavelengths, while the short-wavelength peak (line Peak 1) presents a shift tendency toward long-wavelength direction. As discussed above, there is a transition from the tetragonal to the orthorhombic phase. Thus, we believe that Peak 1 belongs to the orthorhombic phase. A previous study suggested a discontinuity in the crystal structure when $MAPbI_3$ undergoes a phase transition from the high-temperature tetragonal phase to the low-temperature orthorhombic phase, creating new energetic states[16]. Thus, we attributed the PL signal of Peak 2 at the temperature below 160 K to the new states in the orthorhombic phase, where carriers would recombine and emit PL with long wavelengths.

We also conducted temperature-dependent PL measurements for $FAPbI_3$ film and summarized the data [Figure 3]. Colorful mapping of the normalized PL spectra in different temperatures is shown in Figure 3C. The central positions and full width of half maximum of the excitonic peaks are extracted and given in Figure 2D and Supplementary Figure 3. As the temperature decreases, the peak exhibits an apparent shift

tendency towards longer wavelengths and a decrease in full width at half maximum (FWHM), displaying the evolution of the free exciton with temperature[17]. Such shift tendency observed in position from 290 to 160 K is consistent with the evolving band gap calculated in Figure 2D. Compared with $MAPbI_3$, $FAPbI_3$ perovskite shows a simpler evolution tendency owing to its more stable crystal structure.

We further scrutinized the detailed connection between the PL signal and the perovskite structure. As reported, the integrated PL intensity can be fitted by Arrhenius equations with two thermal activation energies, E_1 and E_2, as

$$I(T) = \frac{I_0}{1 + C_1 \exp\left(-\frac{E_1}{k_B T}\right) + C_2 \exp\left(-\frac{E_2}{k_B T}\right)} \quad (1)$$

where $I(T)$ and I_0 are the integrated intensities at T and 0 K. C_1 and C_2 are constants. The reciprocal of integrated PL intensities for $FAPbI_3$ perovskite in different temperatures is fitted using Equation (1) and plotted in Supplementary Figure 4. Then, thermal activation energies E_1 and E_2 are extracted as 441.7 and 17.6 meV, respectively, showing a high correlation with a R^2 of 0.99844. It is reported that E_1 and E_2, virtually representing exciton binding energies in various phases, can be approximately attributed to the activation energies for cubic and tetragonal perovskite phases. Meanwhile, they are also sensitive to the synthesis, composition, and structure details[18]. As shown in Figure 3D, a temperature-dependent trend of the peak positions indicates a smaller binding energy of excitons when the temperature is higher than 160 K. The featuring peak position shows a temperature-independent tendency due to the easy formation of exciton complexes from photoexcited carriers at extremely low temperatures. Thus, we can witness apparent sharp peaks in the low-temperature range in Figure 2C. The changed crystal phase as tetragonal (II) would be responsible for the higher exciton binding energy.

Undoubtedly, the evolved exciton dynamics in varying temperatures has a central role in determining the photovoltaic performance of PSCs. For example, the change of exciton binding energy might affect the separation of electron and hole and then the IV performance. A lower binding energy would be favorable. According to the above results indicating that excitons at a temperature higher than 150 K have a smaller binding energy, we study the photovoltaic performance of whole PSCs by conducting the J-V measurements from 293 to 153 K in a step of 10 K. The PSCs had an ITO/SnO_2/perovskite/Spiro-OMeTAD/Au structure where $FAPbI_3$ and $MAPbI_3$ were used as the light absorber. The obtained PCE, fill factor (FF), V_{OC}, and J_{SC} of the $MAPbI_3$- and $FAPbI_3$-based PSCs are recorded in Figure 4A-D.

In $MAPbI_3$-based PSCs, J_{SC} is stabilized at 20 mA in the 290 to 180K range and starts to decrease rapidly below 180 K. V_{OC} rises continuously before 180 K and then falls sharply. FF remains essentially constant at first and shows a downward trend below 250 K. Considering that the photovoltaic parameters are satisfied by

$$PCE = FF \times Voc \times Jsc \quad (2)$$

The evolution of FF primarily determines the performance change of MAPI-based PSCs at low temperatures. At the temperature range of 250 to 280 K, PCE reaches a high level with a champion value of 17.21%, an improvement of nearly 5% compared to that at room temperature (290 K). In $FAPbI_3$-based

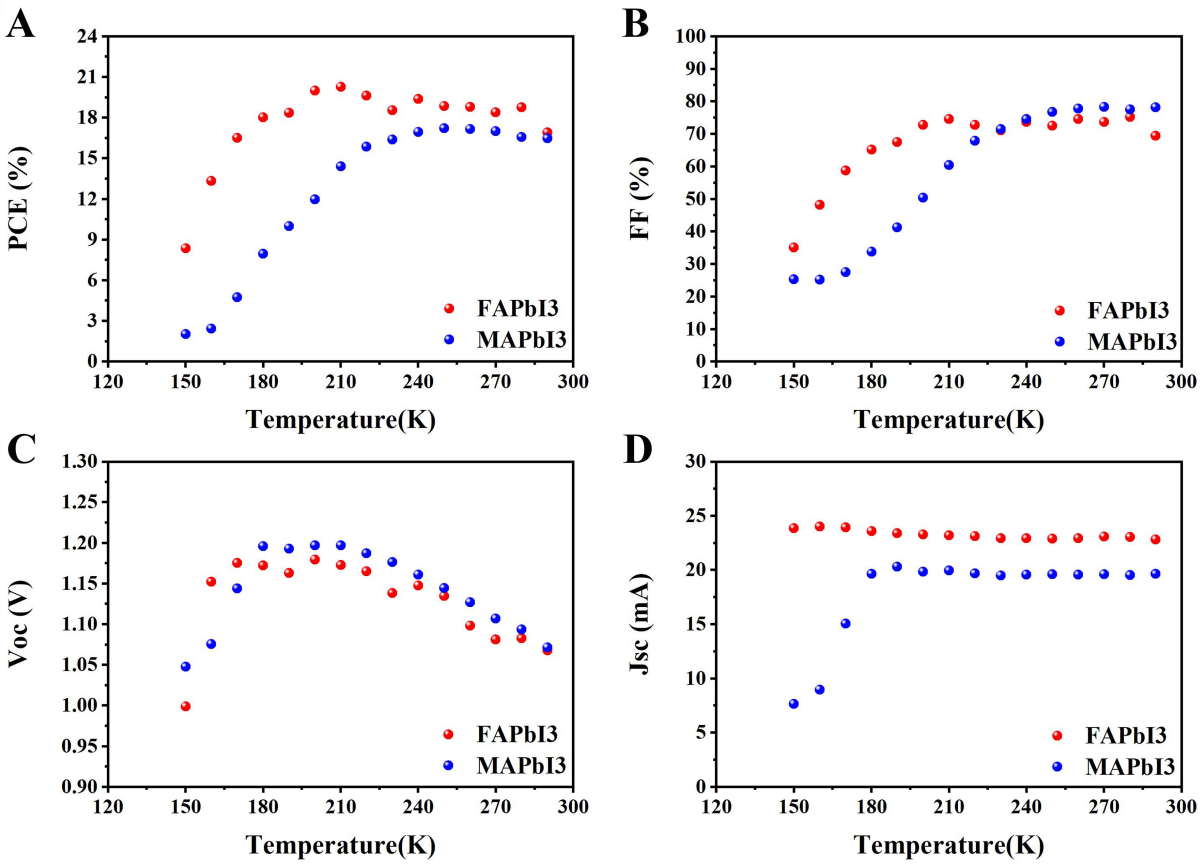

Figure 4. The photovoltaic performance of $MAPbI_3$-based PSCs (blue points) and $FAPbI_3$-based PSCs (red points) from 290 to 150 K: (A) PCE; (B) FF; (C) V_{OC}; and (D) J_{SC}. PSCs: Perovskite solar cells; PCE: power conversion efficiency; FF: fill factor; V_{OC}: open-circuit voltage; J_{SC}: short-circuit current.

PSCs, PCEs show a similar trend that they were mainly affected by FF. FF remains almost the same when the temperature exceeds 210 K. J_{SC} is always stabilized in the full range, while V_{OC} rises continuously before 210 K and then falls sharply. As a result, PCE reaches a best efficiency of 20.28% at 210 K, a nearly 20% increase compared to the control efficiency at room temperature, and then decreases fast.

Next, we tried to use a diode model to scrutinize the change of photovoltaic parameters with the decreasing temperature. Previous works pointed out that the J-V characteristics of thin-film PSC can be determined by a single-exponential diode equation[19,20], expressed as

$$J = J_0 \exp\left[\frac{q}{AkT}(V - RJ)\right] + GV - J_{SC} \quad (3)$$

where R is the series resistance, and G is the parallel conductance, respectively representing losses in the series and parallel circuit model. A stands for the diode ideal factor. The diode reverse current saturation density J_0 can be calculated by

$$J_0 = J_{00} \exp(-\frac{E_A}{AkT}) \quad (4)$$

where E_A is the activating energy (or barrier height) of the main recombination mechanism, and J_{00} is the pre-exponential factor of J_0, which is virtually temperature-independent. Given $G << J_{SC}/V_{OC}$, the expression of V_{OC} can be obtained, by combining Equations (3) and (4), as

$$V_{OC} = \frac{E_A}{q} - \frac{AkT}{q} \ln\left(\frac{J_{00}}{J_{SC}}\right) \quad (5)$$

where the charge q, ideal factor A, Boltzmann's constant k, and J_{00} are constants.

In Figure 4D, J_{SC} of two PSCs is almost unchanged when the temperature is higher than 180 K. Thus, V_{OC} would be a linear function of the temperature T and rise as the temperature decreases. We linearly fitted V_{OC} with temperature for $MAPbI_3$-based and $FAPbI_3$-based PSCs from 290 to 210 K. The results are given in Supplementary Figures 5 and 6. The fitted R^2 for $MAPbI_3$ and $FAPbI_3$ are separately 0.99 and 0.95, revealing a high correlation. That means the perovskites are stable in the temperature range with a relatively stable semiconductor property, consistent with the optical and PL measurement results.

In addition, the E_A value can also be used to indicate the recombination type of perovskite films. If E_A nearly equals E_g, it suggests the recombination in the perovskite film is dominant; if $E_A < E_g$, it indicates that the interface recombination becomes the main mechanism[21]. We extrapolated the linear segment of the two lines to T = 0 K to calculate the value of E_A of the two perovskite films. The $MAPbI_3$ device shows a fitted E_A of 1.54 ± 0.02 eV and a measured band gap of about 1.57 eV from UV-vis spectra [Figure 2B], indicating a bulk recombination rather than an interfacial recombination. As for the $FAPbI_3$ device, a fitted E_A of 1.47 ± 0.03 eV is close to the measured E_g of 1.50 eV [Figure 2D], also showing a dominant mechanism of bulk recombination in the temperature range from 210 to 290 K.

Additionally, the rapid decline in FF at 200 K for $MAPbI_3$ and at 180 K for $FAPbI_3$ is a major factor contributing to the significant drop in the efficiency of the solar cell devices within those corresponding temperature ranges. Given that we observed that cracks appear in the perovskite film during the cooling process along with voids between grain boundaries and considering that these temperatures are close to the phase transition temperatures of the two types of perovskite materials, we speculate that the decrease in FF may originate from the volume changes caused by the low-temperature phase transition, leading to interlayer mismatch.

Thus, it can be concluded that the PSCs comply with a generalized diode model above 210 K when the perovskite crystal structure is stable. Further decreasing the temperature would cause different evolutions. For the $MAPbI_3$ case, as the phase transition from high-temperature tetragonal to low-temperature orthorhombic starts at about 180 K, optoelectronic properties would be changed simultaneously, impairing the photovoltaic performance. However, for the $FAPbI_3$ case, the negative impact of temperature on the photovoltaic performance shows a considerable delay with the decreasing temperature because the phase transition from the high-temperature tetragonal to the low-temperature tetragonal takes place at 140 K. For both types of samples, the interlayer mismatch caused by the phase transition occurring during the cooling process leads to a decrease in FF, resulting in a significant decline in cell efficiency within the corresponding temperature ranges.

CONCLUSIONS

In conclusion, we have established a correlation between the optical behavior of $MAPbI_3$- and $FAPbI_3$-based perovskite films and the corresponding photovoltaic performance changes in low temperatures. With the decreasing temperature, the optical and PL properties evolved. Both the perovskite films show phase transitions at specific low temperatures, which further influenced the photovoltaic performance of PSCs. Briefly, the $MAPbI_3$-based and $FAPbI_3$-based PSCs exhibit notable efficiency improvements of 5% (from 16.46% to 17.21%) and 20% (from 16.91% to 20.28%), respectively, at temperatures higher than 210 K for $FAPbI_3$ and 250 K for $MAPbI_3$, primarily attributed to the enhanced V_{OC}. Further decreasing the temperature impaired the photovoltaic performance owing to the decreased FF. By combining the conventional diode model simulation and optical measurement results, one can infer that the diminishing efficiency would be attributed to the change of crystal structure, even phase transition, at extremely low temperatures. Our findings not only hold promise for applying PSCs in more low-temperature scenarios but also show some instructions to improve the photovoltaic performance of PSCs in extremely low temperatures.

DECLARATIONS

Authors' contributions

Conceived the idea of this study and designed the experiments, fabricated the perovskite films and solar cells, performed the material synthesis, contributed to the SEM, UV-vis and PL characterization, tested the photovoltaic performances: Xu Y, Wu Z

Analyzed the data and wrote the paper: Xu Y, Wu Z, Zhang Z

Supervised this project: Lin H, Li X

Availability of data and materials

The data that support the findings of this study are available from the corresponding author upon reasonable request.

Financial support and sponsorship

This work was financially supported by the National Natural Science Foundation of China (NSFC52072207, 62175204), Science and Technology Project of Fujian Province (No. 2021H6018).

Conflicts of interest

All authors declared that there are no conflicts of interest.

Ethical approval and consent to participate

Not applicable.

Consent for publication

Not applicable.

Copyright

© The Author(s) 2024.

REFERENCES

1. Zhao D, Yu Y, Wang C, et al. Low-bandgap mixed tin-lead iodide perovskite absorbers with long carrier lifetimes for all-perovskite tandem solar cells. *Nat Energy* 2017;2:17018. DOI

2. Weber D. $CH_3NH_3PbX_3$, ein Pb(II)-system mit kubischer perowskitstruktur/$CH_3NH_3PbX_3$, a Pb(II)-system with cubic perovskite structure. *Zeitschrift für Naturforschung B* 1978;33:1443-5. DOI
3. Min H, Lee DY, Kim J, et al. Perovskite solar cells with atomically coherent interlayers on SnO- electrodes. *Nature* 2021;598:444-50. DOI PubMed
4. Xia Y, Zhu M, Qin L, et al. Organic-inorganic hybrid quasi-2D perovskites incorporated with fluorinated additives for efficient and stable four-terminal tandem solar cells. *Energy Mater* 2023;3:300004. DOI
5. Lu YN, Zhong JX, Yu Y, et al. Constructing an n/n^+ homojunction in a monolithic perovskite film for boosting charge collection in inverted perovskite photovoltaics. *Energy Environ Sci* 2021;14:4048-58. DOI
6. Sasaki K, Agui T, Nakaido K, Takahashi N, Onitsuka R, Takamoto T. Development of InGaP/GaAs/InGaAs inverted triple junction concentrator solar cells. *AIP Conf Proc* 2013;1556:22-5. DOI
7. Haase F, Hollemann C, Schäfer S, et al. Laser contact openings for local poly-Si-metal contacts enabling 26.1%-efficient POLO-IBC solar cells. *Sol Energy Mater Sol Cells* 2018;186:184-93. DOI
8. Chen Y, Tan S, Li N, et al. Self-elimination of intrinsic defects improves the low-temperature performance of perovskite photovoltaics. *Joule* 2020;4:1961-76. DOI
9. Izydorczyk W, Waczyński K, Izydorczyk J, et al. Electrical and optical properties of spin-coated SnO_2 nanofilms. *Mater Sci Pol* 2014;32:729-36. DOI
10. D'Innocenzo V, Grancini G, Alcocer MJ, et al. Excitons versus free charges in organo-lead tri-halide perovskites. *Nat Commun* 2014;5:3586. DOI PubMed
11. Kim H, Hunger J, Cánovas E, et al. Direct observation of mode-specific phonon-band gap coupling in methylammonium lead halide perovskites. *Nat Commun* 2017;8:687. DOI PubMed PMC
12. Manoogian A, Woolley JC. Temperature dependence of the energy gap in semiconductors. *Can J Phys* 1984;62:285-7. DOI
13. Geng W, Zhang L, Zhang Y, Lau W, Liu L. First-principles study of lead iodide perovskite tetragonal and orthorhombic phases for photovoltaics. *J Phys Chem C* 2014;118:19565-71. DOI
14. Umebayashi T, Asai K, Kondo T, Nakao A. Electronic structures of lead iodide based low-dimensional crystals. *Phys Rev B* 2003;67:155405. DOI
15. Dai J, Zheng H, Zhu C, Lu J, Xu C. Comparative investigation on temperature-dependent photoluminescence of $CH_3NH_3PbBr_3$ and $CH(NH_2)_2PbBr_3$ microstructures. *J Mater Chem C* 2016;4:4408-13. DOI
16. Baikie T, Fang Y, Kadro JM, et al. Synthesis and crystal chemistry of the hybrid perovskite $(CH_3NH_3)PbI_3$ for solid-state sensitised solar cell applications. *J Mater Chem A* 2013;1:5628-41. DOI
17. Francisco-lópez A, Charles B, Alonso MI, et al. Phase diagram of methylammonium/formamidinium lead iodide perovskite solid solutions from temperature-dependent photoluminescence and raman spectroscopies. *J Phys Chem C* 2020;124:3448-58. DOI
18. Wu K, Bera A, Ma C, et al. Temperature-dependent excitonic photoluminescence of hybrid organometal halide perovskite films. *Phys Chem Chem Phys* 2014;16:22476-81. DOI
19. Phillips JE, Birkmire RW, Mccandless BE, Meyers PV, Shafarman WN. Polycrystalline heterojunction solar cells: a device perspective. *Physica Status Solidi* 1996;194:31-9. DOI
20. Hegedus SS, Shafarman WN. Thin-film solar cells: device measurements and analysis. *Prog Photovolt* 2004;12:155-76. DOI
21. Li Y, Zhuang D, Zhao M, et al. Study on the performance of oxygen-rich Zn(O,S) buffers fabricated by sputtering deposition and Zn(O,S)/Cu(In,Ga)$(S,Se)_2$ interfaces. *ACS Appl Mater Interfaces* 2022;14:24435-46. DOI PubMed